CAMBRIDGE
UNIVERSITY PRESS

Article

Complex hydrogen bonding and thermal behaviour over a wide temperature range of kainite KMg(SO$_4$)Cl·2.75H$_2$O

Artem S. Borisov[1,2], Oleg I. Siidra[1,2]* , Valery L. Ugolkov[2], Alexey N. Kuznetsov[3,4] , Vera A. Firsova[2],

Dmitri O. Charkin[4], Natalia V. Platonova[5] and Igor V. Pekov[6]

[1]Department of Crystallography, St. Petersburg State University, University emb. 7/9, 199034, St. Petersburg, Russia; [2]Institute of Silicate Chemistry, Russian Academy of Sciences, Adm. Makarova emb. 2, 199034, St. Petersburg, Russia; [3]Kurnakov Institute of General and Inorganic Chemistry RAS, Leninskii prosp., 31, 119991, Moscow, Russia; [4]Department of Inorganic Chemistry, Faculty of Chemistry, Moscow State University, Vorobievy Gory, 119991, Moscow, Russia; [5]X-ray Diffraction Resource Center, St. Petersburg State University, University emb. 7/9, 199034, St. Petersburg, Russia; and [6]Department of Mineralogy, Faculty of Geology, Moscow State University, Vorobievy Gory, 119991, Moscow, Russia

Abstract

Kainite, KMg(SO$_4$)Cl·2.75H$_2$O, is one of the most common hydrated sulfate minerals, and it plays an important role as a source of potassium. However, its properties and structure have, to date, been insufficiently studied. In our present work, kainite was investigated using multiple techniques, including single-crystal and powder X-ray diffraction, thermogravimetry, differential scanning calorimetry (DSC), and infrared spectroscopy (IR). The mineral is monoclinic, $C2/m$, $a = 19.6742(2)$, $b = 16.18240(10)$, $c = 9.49140(10)$ Å, $\beta = 94.8840(10)°$, $V = 3010.86(5)$ Å^3 and $Z = 16$. The structure was refined to $R_1 = 0.0230$ for 3080 unique observed reflections with $|F_o| \geq 4\sigma F$. The complex hydrogen bonding system for kainite is described for the first time. The structure of kainite contains seven symmetrically independent sites occupied by water molecules, six of which are strongly bonded to Mg^{2+} cations while the seventh resides in the framework cavities. The acceptors of the hydrogen bonds are either chloride anions, neighbouring water molecules or oxygens atoms of sulfate groups. A bifurcated hydrogen bond was described for one of the water molecules. Based on the analysis of the crystal structure, we have confirmed and propose the correct formula for kainite as KMg(SO$_4$)Cl·2.75H$_2$O. The thermal studies of kainite in the temperature range of –150°C to +600°C indicate its stability to 190°C. The decomposition products are K$_2$Mg$_2$(SO$_4$)$_3$, KCl and K$_2$SO$_4$. The thermal expansion was calculated, which for kainite has a character typical for monoclinic crystals and similar to the compressibility tensor described earlier.

Keywords: kainite, sulfates, X-ray diffraction, hydrogen bonding, bifurcated hydrogen bond, thermal expansion

Introduction

Hydrated sulfates are the most common and important minerals of evaporite deposits (Jena, 2021). Kainite, KMg(SO$_4$)Cl·2.75H$_2$O (Zincken, 1865; Robinson *et al.*, 1972), is an essential potassium concentrator in this formation, as well as an important potassium ore along with sylvite KCl, carnallite KMgCl$_3$·6H$_2$O, langbeinite K$_2$Mg$_2$(SO$_4$)$_3$ and polyhalite K$_2$Ca$_2$Mg(SO$_4$)$_4$·2H$_2$O (Spencer, 2000; Babel and Schreiber, 2014; Jena, 2021). As the most important potassium deposits are connected with evaporites, the flotation properties of potassium minerals, including complex potassium salts and kainite in particular, have been studied (Miller and Yalamanchili, 1994; Hancer and Miller, 2000). Lately, much attention has been paid to the evaporite weathering processes (Censi *et al.*, 2016), which are of essential ecological concern in the environment of salt-bearing deposits (Wang *et al.*, 2019); possible effects on climate changes have also been discussed recently (Warren, 2010; Shields and Mills, 2021). In

addition, kainite is of interest for isotopic studies as it also contains both sulfur (Hryniv *et al.*, 2007) and chlorine (Eggenkamp *et al.*, 1995).

The K–Mg–SO$_4$–Cl system has been studied thoroughly, including both thermodynamic and phase relationships (Jänecke, 1912), as well as polythermic studies (Campbell *et al.*, 1934; Eugster *et al.*, 1980; Abdel Wahed *et al.*, 2015). The phase relationships of kainite with other sulfate minerals of evaporites are listed in Braitsch (1971). The first pathway of kainite formation includes incongruent melting of carnallite, KMgCl$_3$·6H$_2$O, in MgSO$_4$-bearing systems. This is the most important hypergenic process in transformations of potassium salts (Braitsch, 1971). In these systems, carnallite melts below 72°C; in the presence of kieserite, MgSO$_4$·H$_2$O, the main reaction product is kainite. The second pathway is direct reaction of kieserite with sylvite in a NaCl solution. The kieserite–sylvite paragenesis in the MgSO$_4$-bearing systems takes place above 72°C (Braitsch, 1971). Yet, there exist two boundary conditions which need to be considered. The first one is excess kieserite which reacts with NaCl solution forming löweite and blödite. In their presence, kainite slowly dissolves with formation of leonite and 'glazerite' (aphtitalite) (Braitsch, 1971). The second one is the presence of excess sylvite, which however can coexist with kainite. Further reaction with

NaCl solution also leads to the formation of leonite and aphtitalite but not blödite (Braitsch, 1971).

Kainite has also been detected among the products of interaction between fumarolic exhalations and moist air. For instance, in the fumaroles of Tolbachik volcano, Kamchatka, Russia, it is observed in the relatively low-temperature (50–150°C) sulfate–chloride zones which contain a variety of hydrated minerals. In the hotter (>200°C) sulfate–oxide zone, only anhydrous species are stable (Pekov *et al.*, 2015). In respect of high-temperature mineral associations, there remains an open question of 'anhydrokainite' KMg(SO$_4$)Cl (Jänecke, 1912; Kassner, 1958 and references therein).

Several attempts have been made to prepare synthetic kainite doped by various magnetically active cations, namely Mn^{2+}, Cu^{2+}, Cr^{3+}, VO^{2+}, Co^{2+} and Ni^{2+} (e.g. Subramanian and Hariharan, 1986; Narasimhulu *et al.*, 2000; Dhanuskodi and Jeyakumari, 2001, 2004; Rao *et al.*, 1994), and their studies using nuclear magnetic resonance. Structural characterisation of sulfate anions in the structure of kainite were also supported by spectroscopic studies (Murthy *et al.*, 1992a, 1992b; Salagram *et al.*, 1988, 1994). In addition, natural kainite is a proper object for investigating crystal chemical behaviour of chloride anions which coordinate to cations, including high-pressure studies (Nazzareni *et al.*, 2018).

Despite numerous studies of kainite, its thermal expansion has not been investigated. The description of its thermal behaviour (Bish and Scanlan, 2006) reports only decomposition points (60°C *in vacuo* and 80°C under ambient conditions), while the nature of decomposition products remains unaddressed (note the proposed 'anhydrokainite' which is also not characterised).

In the current study, we investigated the thermal behaviour of kainite using thermogravimetry methods (TG and DTG), differential scanning calorimetry (DSC), and variable-temperature powder X-ray diffraction (XRD). The thermal expansion of kainite was studied based on the XRD results in the –150°C to 50°C temperature range. These results are of particular interest as they cover natural terrestrial conditions, including those in rich evaporite deposits.

According to the International Mineralogical Association approved list of minerals (Pasero, 2022), the formula of kainite is KMg(SO$_4$)Cl·3H$_2$O. The crystallochemically correct formula is KMg(SO$_4$)Cl·2.75H$_2$O, based on the refined water content (Robinson *et al.*, 1972). Our results (*vide infra*) confirm the latter formulation. Therefore, we propose KMg(SO$_4$)Cl·2.75H$_2$O as the most correct one.

It is worth noting that kainite may exist also on the Martian surface in the Gusev crater (Rice *et al.*, 2010). The results of thermal studies of kainite may be helpful in understanding the behaviour of the compound analogous to the extra-terrestrial one. Note that the surface temperature of Mars varies from –150°C to 10–20°C (Barlow, 2008, and references therein). The temperature range in our study partially overlaps with the latter.

Experimental

Sample description

The sample of kainite studied originates from the old potassium salt deposit Wilhelmshall located near the city of Halberstadt, Saxony-Anhalt, Germany. The material for studies was separated from a transparent, colourless tabular large (1.5 cm × 4 cm × 5 cm) single crystal of kainite collected in the first quarter of the 20th Century from the underground mine.

Table 1. Crystallographic data and refinement parameters for studied kainite.

Crystal data:	
Temperature (K)	100
Radiation	Cu*K*α, 1.54184 Å
Crystal system	monoclinic
Space group	*C*2/*m*
a (Å)	19.6742(2)
b (Å)	16.18240(10)
c (Å)	9.49140(10)
β (°)	94.8840(10)
Volume (Å^3) / *Z*	3010.86(5) / 16
D_{calc} (g/cm^3)	2.157
μ (mm^{-1})	12.900
Crystal size (mm)	0.14 × 0.10 × 0.05
Data collection:	
θ range (°)	3.542–76.954
h, *k*, *l* ranges	–24 → 24, –20 → 18, –11 → 11
Total reflections collected	12,153
Unique reflections (R_{int})	3169 (0.0263)
Unique reflections $F > 4σF$	3080
Structure refinement:	
Weighting scheme *a*, *b*	0.0376, 3.7245
Extinction coefficient	0.000140(18)
$R_1[F > 4σ_F]$, $wR_2[F > 4σ_F]$	0.0230, 0.0652
R_1 all, wR_2 all	0.0235, 0.0656
Goodness-of-fit	1.074
Largest diff. peak and hole (e$^-$ Å^{-3})	0.566, –0.638

Electron microprobe study

Semi-quantitative electron-microprobe analysis (EMPA) was carried out using a JXA 850A scanning electron microscope equipped with a LINK 1000 energy-dispersive spectrometer. The energy dispersive spectroscopy mode was used, with an acceleration voltage of 20 kV, a beam current of 2 nA and a 5 μm beam diameter. The EMPA data showed the presence of significant amounts of K, Mg, S, Cl and O in the mineral. Contents of other elements with atomic numbers higher than that of oxygen are below their detection limits.

Single-crystal studies

The crystals of kainite were examined under an optical microscope and a suitable one selected and mounted on glass fibre for the data collection. The single-crystal X-ray data collection was carried out using a XtaLAB Synergy diffractometer with a micro-focus sealed X-ray tube (Cu*K*α radiation) operating at 50 kV and 1.0 mA in an ambient N$_2$ atmosphere at 100 K, with frame widths of 0.5° and a 0.15–0.40 s count for each frame (based on calculated strategy). The data were integrated and corrected by means of the *CrysAlisPro* 1.171.41.103a (Rigaku, 2021) program package, which was also used to apply an empirical absorption correction using spherical harmonics, as implemented in the *SCALE3 ABSPACK* scaling algorithm. The *SHELXL* program (Sheldrick, 2015) was used for the crystal-structure refinement. The structure was refined to $R_1 = 0.023$ for 3080 unique observed reflections with $|F_o| \geq 4σF$. All experimental details are given in Table 1. The crystallographic information files have been deposited with the Principal Editor of *Mineralogical Magazine* and are available as Supplementary material (see below).

As an initial structure model, the atomic coordinates of K, Mg, S, Cl and O atoms were taken from Robinson *et al.* (1972). All of the subgroups of the *C*2/*m* space group were tried but none of them led to better refinement results for the positions of hydrogen atoms

Table 2. Coordinates and atomic displacement parameters (Å^2) of non-hydrogen atoms in the crystal structure of kainite.

Site	Wyck. position	x	y	z	U_{eq}	U^{11}	U^{22}	U^{33}	U^{23}	U^{13}	U^{12}
K1	4i	0.19146(2)	½	0.41940(5)	0.00972(12)	0.0086(2)	0.0101(2)	0.0108(2)	0	0.00303(18)	0
K2	4i	0.19274(2)	0	0.93944(5)	0.00870(11)	0.0079(2)	0.0091(2)	0.0094(2)	0	0.00215(17)	0
K3	8j	0.19459(2)	0.30633(2)	0.84773(4)	0.01079(10)	0.00961(17)	0.01477(19)	0.00804(17)	−0.00005(13)	0.00105(12)	−0.00289(13)
Mg1	2d	0	½	½	0.0056(2)	0.0043(4)	0.0061(5)	0.0064(5)	0	0.0011(4)	0
Mg2	2a	0	0	0	0.0060(2)	0.0052(5)	0.0063(5)	0.0066(5)	0	0.0015(4)	0
Mg3	4f	¼	¼	½	0.00650(16)	0.0054(3)	0.0070(4)	0.0072(3)	0.0000(3)	0.0017(3)	0.0006(3)
Mg4	8j	0.00014(2)	0.24850(3)	0.24822(5)	0.00590(13)	0.0051(3)	0.0074(3)	0.0053(3)	−0.0005(2)	0.0006(2)	0.0002(2)
S1	8j	0.09713(2)	0.33123(2)	0.51696(4)	0.00498(10)	0.00396(18)	0.0060(2)	0.00497(19)	0.00014(13)	0.00056(13)	0.00030(13)
S2	8j	−0.09851(2)	0.16750(2)	−0.01353(4)	0.00515(10)	0.00431(18)	0.0062(2)	0.00502(19)	0.00004(13)	0.00069(13)	0.00003(13)
Cl1	4i	0.21237(3)	0	0.27354(6)	0.01229(13)	0.0153(3)	0.0112(3)	0.0105(3)	0	0.0013(2)	0
Cl2	4i	0.13966(3)	0	0.62304(6)	0.01103(12)	0.0102(2)	0.0109(3)	0.0121(3)	0	0.00190(19)	0
Cl3	8j	0.17902(2)	0.38978(3)	0.13560(4)	0.01358(11)	0.00884(18)	0.0162(2)	0.0160(2)	−0.00495(15)	0.00302(14)	−0.00235(14)
O1	8j	0.07142(5)	0.23267(7)	0.91539(12)	0.0081(2)	0.0075(5)	0.0086(5)	0.0079(5)	0.0012(4)	−0.0002(4)	0.0002(4)
O2	8j	0.07127(5)	0.26847(7)	0.41419(12)	0.0087(2)	0.0074(5)	0.0100(6)	0.0084(5)	−0.0017(4)	−0.0004(4)	0.0000(4)
O3	8j	0.07516(6)	0.31213(7)	0.65747(12)	0.0087(2)	0.0081(5)	0.0121(6)	0.0063(5)	0.0009(4)	0.0023(4)	−0.0016(4)
O4	8j	0.07351(6)	0.41410(7)	0.47141(12)	0.0084(2)	0.0077(5)	0.0077(5)	0.0102(5)	0.0017(4)	0.0022(4)	0.0022(4)
O5	8j	0.07163(6)	0.08636(7)	0.96308(12)	0.0082(2)	0.0085(5)	0.0065(5)	0.0097(5)	−0.0015(4)	0.0020(4)	−0.0011(4)
O6	8j	0.07652(6)	0.18429(7)	0.15636(12)	0.0081(2)	0.0076(5)	0.0106(6)	0.0063(5)	−0.0010(4)	0.0018(4)	0.0013(4)
O7	8j	0.17258(5)	0.33261(7)	0.52621(12)	0.0074(2)	0.0049(5)	0.0072(5)	0.0100(5)	−0.0004(4)	0.0009(4)	0.0005(4)
O8	8j	0.17301(5)	0.16660(7)	0.01779(12)	0.0080(2)	0.0052(5)	0.0097(6)	0.0093(5)	0.0006(4)	0.0008(4)	0.0004(4)
Ow1	4i	0.04007(8)	0	0.21913(17)	0.0095(3)	0.0095(7)	0.0113(8)	0.0079(7)	0	0.0018(6)	0
Ow2	4i	0.02095(8)	½	0.71999(17)	0.0091(3)	0.0089(7)	0.0111(8)	0.0073(8)	0	0.0008(6)	0
Ow3	8j	0.21256(6)	0.17391(7)	0.65194(13)	0.0124(2)	0.0120(6)	0.0111(6)	0.0145(6)	0.0033(5)	0.0032(4)	0.0001(4)
Ow4	8j	0.02579(6)	0.35847(7)	0.14657(12)	0.0088(2)	0.0082(5)	0.0085(5)	0.0098(5)	−0.0004(4)	0.0019(4)	0.0000(4)
Ow5	8j	0.01978(6)	0.13549(7)	0.64843(12)	0.0096(2)	0.0088(5)	0.0096(6)	0.0104(5)	−0.0002(4)	0.0013(4)	0.0020(4)
Ow6	8j	0.19665(6)	0.18599(8)	0.34253(13)	0.0107(2)	0.0078(5)	0.0115(6)	0.0124(6)	−0.0030(5)	−0.0020(4)	0.0017(4)
Ow7	4i	0.14690(10)	½	0.8420(2)	0.0434(7)	0.0126(9)	0.106(2)	0.0111(10)	0	−0.0012(8)	0

than those reported below. All H atoms were located from the analysis of difference-Fourier electron density maps and were refined with the imposed O–H distance restraints of 1.00 ± 0.005 Å and for H2a–H2b with restraints of 1.65 ± 0.05 Å. The isotropic displacement parameters for hydrogen atoms were held constant at 0.065 Å^2. H1B···H5B and H2B···H4B distances are relatively short, whereas their elongation and restraining result in strong distortions of the geometry of the water molecules. A slightly larger U_{eq} value for the Ow7 atom of the water molecule (Table 2) can be explained by the fact that it belongs to the interstitial $(H_2O)^0$ group.

Density functional theory calculations

Density functional theory (DFT) calculations on the equilibrium structure of kainite were undertaken utilising the Projector Augmented Wave method (PAW) as implemented in the pseudopotential *Vienna Ab initio Simulation Package* (VASP) code (Kresse and Joubert, 1999; Kresse and Furthmüller, 2017). Constrained structure optimisation was performed, retaining the unit cell metrics and allowing full atomic coordinate relaxation. To accommodate the procedure, an experimentally established structure was transformed to the *P*1 space group and used as a starting model. The MetaGGA-type SCAN exchange-correlation functional (Sun *et al.*, 2015) was used in the calculations. The energy cut-off was set at 500 eV with a $6 \times 6 \times 12$ gamma-centred *k*-point mesh used for Brillouin zone sampling. The convergence criterion for the procedure was set at 5×10^{-3} meV. Optimised coordinates of the hydrogen atoms are compared to those derived from the XRD experiment in Table 3. The geometrical parameters of the experimentally and theoretically derived hydrogen bonding systems are compared in Table 4. In fact, very good agreement between the XRD data and DFT

Table 3. Coordinates of the H sites in the crystal structure of kainite determined by X-ray diffraction (XRD) analysis and density functional theory (DFT) calculations.

Site	Method	x	y	z
H1a	XRD	0.0910(3)	0	0.231(5)
	DFT	0.10629	0	0.29266
H1b	XRD	0.014(2)	0	0.305(3)
	DFT	0.01481	0	0.34265
H2a	XRD	0.0706(6)	½	0.753(5)
	DFT	0.07846	½	0.75608
H2b	XRD	0.000(2)	½	0.812(2)
	DFT	0.00323	½	0.79195
H3a	XRD	0.2469(12)	0.150(2)	0.724(3)
	DFT	0.24773	0.15319	0.72868
H3b	XRD	0.1823(14)	0.1249(13)	0.634(4)
	DFT	0.18279	0.12707	0.63184
H4a	XRD	0.0758(4)	0.365(2)	0.140(4)
	DFT	0.07449	0.35855	0.13033
H4b	XRD	0.0040(16)	0.4039(15)	0.198(3)
	DFT	0.00455	0.40817	0.2018
H5a	XRD	0.0646(9)	0.1068(19)	0.651(4)
	DFT	0.06571	0.10093	0.67673
H5b	XRD	−0.0084(15)	0.0939(16)	0.695(3)
	DFT	−0.013175	0.08945	0.66321
H6a	XRD	0.2006(17)	0.1254(5)	0.327(3)
	DFT	0.20467	0.12428	0.33248
H6b	XRD	0.1528(9)	0.205(2)	0.293(3)
	DFT	0.1529	0.19533	0.29081
H7a	XRD	0.1921(11)	½	0.801(5)
	DFT	0.19588	½	0.80946
H7b	XRD	0.149(2)	½	0.9473(7)
	DFT	0.15581	½	0.94956

calculations was achieved, which is emphasised by the fact that even calculated hydrogen atom positions, which contribute the least to the total energy, matched the experimental ones very closely. This fact proves our model to be correct.

Table 4. Hydrogen bonding distances (*d* in Å) and angles (°) in kainite (*D* – donor, *A* – acceptor).

D–H···*A*		*d*(*D*–H)	*d*(H···*A*)	<*DHA*	*d*(*D*···A)
Ow1–H1a···Cl1	XRD	0.998(5)	2.388(6)	177(4)	3.3851(17)
	DFT	0.987	2.183	153.62	3.099
Ow2–H2a···Ow7	XRD	1.000(5)	1.658(11)	168(4)	2.644(3)
	DFT	1.000	1.586	172.56	2.581
Ow3–H3b···Cl2	XRD	0.997(5)	2.188(10)	165(3)	3.1601(12)
	DFT	0.983	2.207	159.49	3.147
Ow4–H4a···Cl3	XRD	0.995(5)	2.076(6)	174(3)	3.0673(12)
	DFT	0.986	2.17	151.46	3.072
Ow4–H4b···Ow2[i]	XRD	0.998(5)	1.826(9)	168(3)	2.8096(15)
	DFT	0.991	1.86	169.03	2.839
Ow5–H5a···Cl2	XRD	0.996(5)	2.303(14)	157(3)	3.2442(12)
	DFT	0.977	2.278	158.15	3.205
Ow5–H5b···Ow1[ii]	XRD	0.998(5)	1.858(11)	165(3)	2.8331(16)
	DFT	0.991	1.76	168.84	2.739
Ow6–H6a···Cl1	XRD	0.996(5)	2.109(6)	174(3)	3.1012(12)
	DFT	0.987	2.081	172.03	3.062
Ow6–H6b···O6	XRD	0.993(5)	1.928(18)	149(3)	2.8281(16)
	DFT	0.992	1.757	159.99	2.711
Ow6–H6b···O2	XRD	0.993(5)	2.29(3)	121(2)	2.9351(16)
	DFT	0.992	2.336	116.8	2.92
Ow7–H7a···Cl1[iii]	XRD	0.998(5)	2.066(6)	177(4)	3.064(2)
	DFT	0.99	1.999	174.1	2.985
Ow7–H7b···Cl3[iv]	XRD	0.998(5)	2.560(11)	133.3(11)	3.3238(18)
	DFT	0.981	2.469	135.08	3.239

Symmetry codes: (i) –*x*, –*y*+1, –*z*+1; (ii) –*x*, –*y*, –*z*+1; (iii) –*x*+½, –*y*+½, –*z*+1; (iv) *x*, *y*, *z*+1.

Minor differences between the XRD and DFT results can be assigned to the effect of temperature, as nominal temperature for the results of the DFT calculations is 0 K and the temperature used for the XRD measurements was 100 K.

Infrared spectroscopy

The infrared (IR) spectrum of kainite was acquired on a Bruker Vertex 70 FTIR spectrometer in the 370–4000 cm^{-1} wavelength range (4 cm^{-1}, 32 scans). The powdered sample was mixed with preheated potassium bromide (Sigma-Aldrich, >99.0%) and pressed into a pellet. A similar pellet of pure KBr was used as a reference.

Variable-temperature powder X-ray diffraction

The XRD patterns were registered on a Rigaku Ultima IV powder diffractometer (Rigaku R–300 camera, Cu*K*α radiation for the temperature range –150°C to 50°C and Rigaku HTA 1600 camera, Co*K*α radiation for the 50°C–600°C range, linear PSD detector). The sample was ground thoroughly, suspended in dry heptane, and transferred onto a Pt–Rh holder. The heating rate was 2°C/min. Phase analysis was performed based on the PDF–2 database (powder diffraction file from the International Centre for Diffraction Data, http://www.icdd.com/, accessed 2020), and PDXL (Rigaku, 2016) and *TOPAS V.5.0* (Bruker, 2014) suites. Thermal expansion of kainite was calculated using the *Theta-To-Tensor* (Bubnova *et al.*, 2013) program suite. As different wavelengths were employed in temperature intervals, the powder XRD patterns (Fig. 7) are plotted as *I vs. d*$^{-1}$ (Å^{-1}).

Thermal analysis and mass-spectroscopy

The thermal behaviour of the kainite sample was also investigated on a NETZSCH STA 429 CD thermal analyser using TG+DSC sample holders and Pt/Pt-Rh thermocouples (S type). Heating
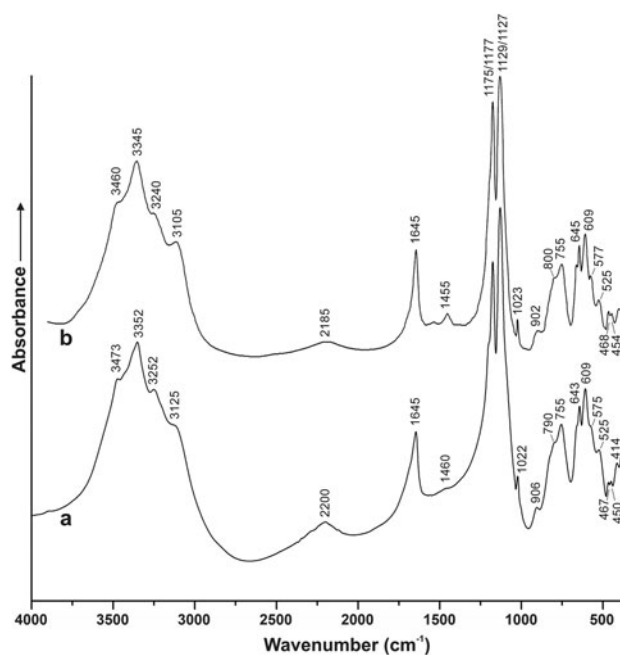
Fig. 1. Infrared (IR) spectra of kainite studied from (a) Wilhelmshall and (b) from its type locality, Brefeld, Tarthun, Stassfurt potash deposit, Saxony-Anhalt, Germany (Chukanov, 2014).

was performed from 35°C to 600°C, while cooling was from 550°C to 200°C with a ramp of 10°C/min in an air flow (50 ml/min). The sample was ground and pressed into a pellet (1 kgf/mm^2). The initial sample weight was 25.23 mg. The pellet was placed in an open alumina crucible. The TG (%) and DSC (mW/mg) data were recorded simultaneously. The sample was photographed *in situ* before and after the heating/cooling cycle.

Results and discussion

Infrared studies

The IR spectrum of the kainite sample is depicted in Fig. 1; it virtually coincides with that registered in Chukanov (2014) for a kainite sample from the type locality. The spectrum contains bands corresponding to the vibrations of sulfate groups and water molecules. Their positions (in cm^{-1}) and assignments are the following: 3473, 3352, 3252 and 3125 [stretching O–H vibrations of water molecules H_2O]; 2200 [proton shift from water molecule to the sulfate anions with formation of HSO_4^-]; 1645 [bending vibrations of H_2O molecules]; 1460 [possibly, bending vibrations of admixed NH_4^+ cations]; 1175 and 1129 [$\nu_3(F_2)$ asymmetric vibrations of SO_4^{2-}]; 1022 [$\nu_1(A_1)$ symmetric vibrations of SO_4^{2-}], 906, 790 and 755 [H_2O and OH libration modes]; 643, 609 and 575 [$\nu_4(F_2)$ of SO_4^{2-}]; 525, 467, 450 and 414 [Mg–O stretching vibrations, $\nu_2(E)$ SO_4^{2-}, and lattice modes involving translation of K$^+$, Cl$^-$ and SO_4^{2-} as a whole].

Crystal structure

The crystal structure of kainite was first determined in Robinson *et al.* (1972). Our refinement allowed us to localise the positions of hydrogen atoms which play an essential role in the structure formation. Refined atomic coordinates are given in Table 2;
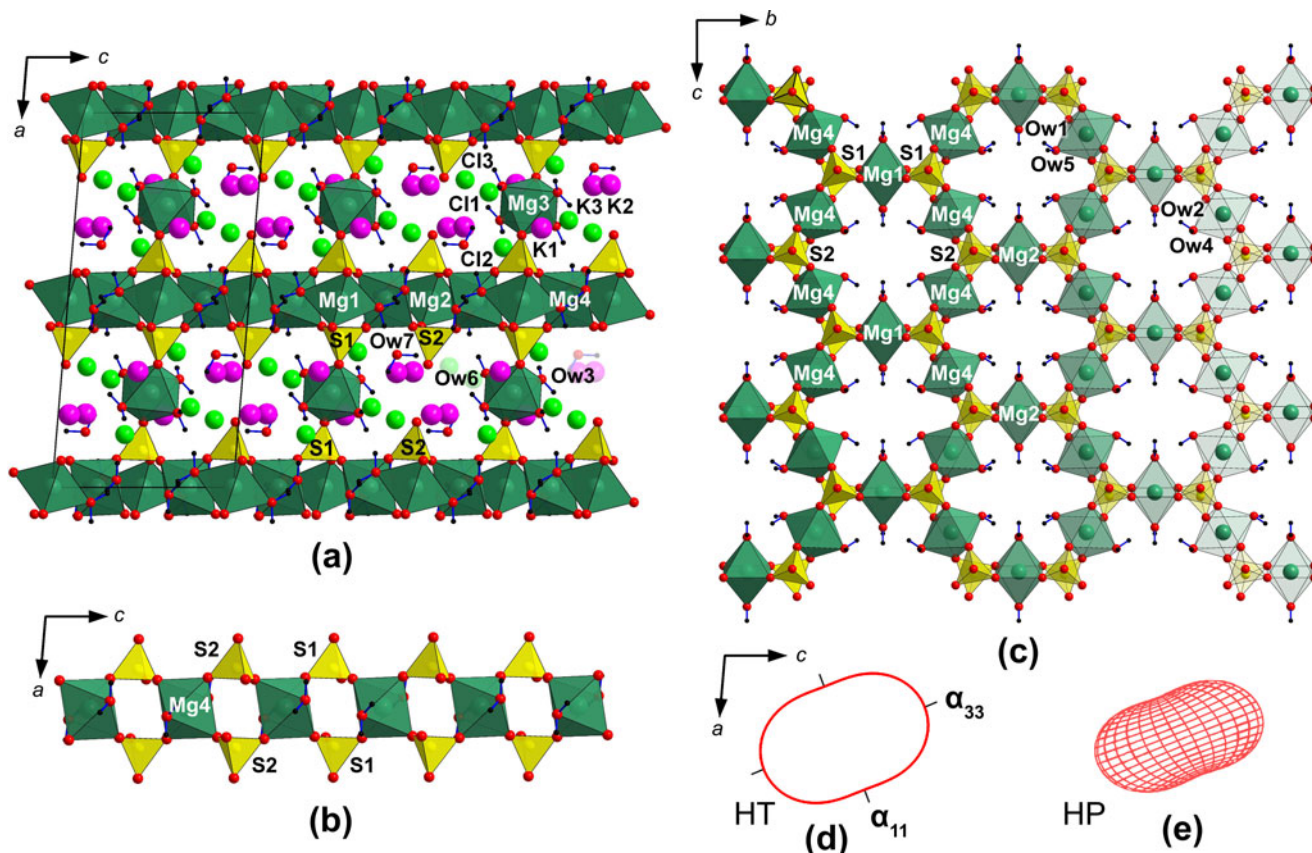
Fig. 2. Crystal structure of kainite along the *b* axis (*a*). Kröhnkite-type chains (*b*) (highlighted by the red dotted line) form layers (*c*) further interconnected via Mg-centred polyhedron into framework. Thermal expansion tensor of the structure of kainite (*d*), and its compressibility tensor (*e*) (after Nazzareni *et al.*, 2018).

Supplementary Table S1 lists the bond-valence sums calculated using parameters given in Gagné and Hawthorne (2015).

The kainite structure (Fig. 2a) can be considered as based on kröhnkite-like chains (Fig. 2b) (Hawthorne *et al.*, 2000; Fleck *et al.*, 2002), comprised of $Mg4O_4(H_2O)_2$ octahedra (Fig. 3) linked by $S1O_4$ and $S2O_4$ sulfate tetrahedra and stretched along *c*. The chains are linked by $Mg1O_4(H_2O)_2$ and $Mg2O_4(H_2O)_2$ species to form layers (Fig. 2c) parallel to (100). Further linkage via $Mg3O_2(H_2O)_4$ assembles these layers into a porous framework. The Mg1, Mg2 and Mg4 adopt the *trans*-$MgO_4(H_2O)_2$ coordination with a basal plane formed by sulfate oxygens and apical vertices, by water molecules. The Mg3 atom is coordinated by two sulfate oxygens and four water molecules. The average Mg–O distances (Table 5) for all $MgO_n(H_2O)_m$ octahedra lie in the range 2.057–2.078 Å which is in a good agreement with the value of 2.089 Å given by Gagné and Hawthorne (2016). The sulfate tetrahedra are close to regular and the mean S–O distances of 1.473 and 1.475 Å for S1 and S2, respectively, almost coincide with the statistical data for sulfates (Hawthorne *et al.*, 2000; Gagné and Hawthorne, 2018). The cavities of the framework also host three independent potassium sites of which K1 and K2 adopt a similar KO_4Cl_4 coordination with the mean values of 2.856 and 2.810Å (K–O) and 3.291 and 3.173 Å (K–Cl) for K1 and K2 (Fig. 3). The K3 site has a different coordination: $KO_5(H_2O)_3Cl$. Based on the description of the crystal structure of kainite given above, we suggest the following crystal chemical formula – $K[Mg(H_2O)_{2.5}(SO_4)]Cl\cdot(H_2O)_{0.25}$. The brackets designate the formula of the framework.

Hydrogen bonding

The structure of kainite contains seven symmetrically independent sites occupied by water molecules (Fig. 4). Ow1, Ow2, Ow3, Ow4, Ow5 and Ow6 water molecules are strongly bonded to Mg^{2+} cations while the Ow7 site resides in the framework cavities. Structural details of the hydrogen bond system are collected in Table 4. The interactions with separations of H···$A < r(A) + 2$ Å and <*DHA* (*D* = donor and *A* = acceptor) above 110° were taken into consideration (Steiner, 2002).

The acceptors of the hydrogen bonds are either chloride anions, neighbouring water molecules or oxygens of sulfate groups (Table 4, Figs 4, 5). The Ow1 water molecule coordinating the Mg2 atom (Fig. 4a) forms only one hydrogen bond through the H1a atom to Cl1 acceptor with the interatomic distance 2.388 Å and the *D*–H····*A* angle 177°. The *D*–H····*A* angle for H1b and Ow5 as a potential acceptor is 109° and does not meet the criteria for hydrogen bonding mentioned above. The Ow2 molecule has a somewhat similar environment (Fig. 4b). The hydrogen atom H2a forms a moderate hydrogen bond to the interstitial Ow7 water molecule. Atom H2b was also excluded from the hydrogen bonding system because of the aforementioned criteria – the Ow2–H2b····Ow4 angle is 105°. The Ow3 water molecule (Fig. 4c) also forms a moderate hydrogen bond via the H3b to Cl2 acceptor.

Both Ow4 and Ow5 water molecules (coordinating Mg4-centered polyhedron) have a similar coordination environment (Figs 4a,b, 5) with both H atoms participating in the hydrogen bonding system. The H4a atom, as well as H5a, have chlorine
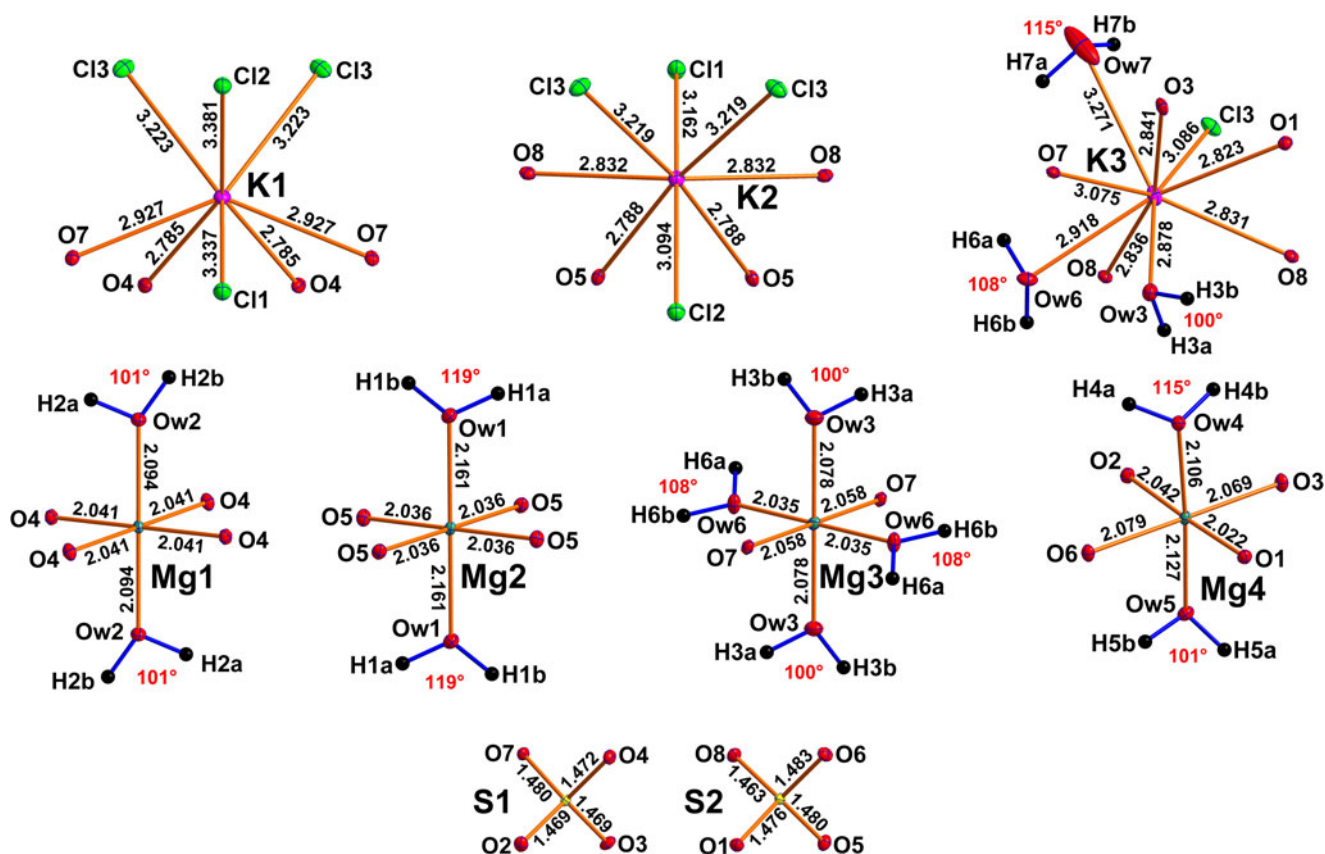
Fig. 3. Coordination of cations in the crystal structure of kainite. All interatomic distances are given in Å. Atomic displacement parameters for ellipsoids are drawn at the 50% probability level.

Table 5. Selected interatomic distances (Å) in kainite.

K1–O4	×2	2.7850(12)	Mg1–O4	×4	2.0406(11)
K1–O7	×2	2.9270(11)	Mg1–Ow2	×2	2.0936(16)
K1–Cl3	×2	3.2225(6)	<Mg1–O>		2.058
K1–Cl1		3.3369(7)			
K1–Cl2		3.3807(7)	Mg2–O5	×4	2.0362(11)
<K1–O>		2.856	Mg2–Ow1	×2	2.1606(16)
<K1–Cl>		3.291	<Mg2–O>		2.078
K2–O5	×2	2.7877(12)	Mg3–Ow6	×2	2.0350(12)
K2–O8	×2	2.8321(12)	Mg3–O7	×2	2.0575(11)
K2–Cl2		3.0943(7)	Mg3–Ow3	×2	2.0782(12)
K2–Cl1		3.1617(7)	<Mg3–O>		2.057
K2–Cl3	×2	3.2188(5)			
<K2–O>		2.810	Mg4–O1		2.0216(12)
<K2–Cl>		3.173	Mg4–O2		2.0419(12)
			Mg4–O3		2.0692(12)
K3–O1		2.8231(12)	Mg4–O6		2.0788(12)
K3–O8		2.8312(12)	Mg4–Ow4		2.1061(13)
K3–O8		2.8355(11)	Mg4–Ow5		2.1273(13)
K3–O3		2.8405(12)	<Mg4–O>		2.074
K3–Ow3		2.8778(13)			
K3–Ow6		2.9176(13)	S1–O2		1.4688(12)
K3–O7		3.0750(12)	S1–O3		1.4694(12)
K3–Cl3		3.0864(5)	S1–O4		1.4720(12)
K3–Ow7		3.2706(7)	S1–O7		1.4798(11)
<K3–O>		2.934	<S1–O>		1.473
<K3–Cl>		3.086			
			S2–O8		1.4629(11)
			S2–O1		1.4762(12)
			S2–O5		1.4798(12)
			S2–O6		1.4828(11)
			<S2–O>		1.475

atoms as acceptors with distances of 2.076 Å for H4a····Cl3 and 2.303 Å for H5a····Cl2, and bond-valence values of 0.27 and 0.18 valence units, respectively. Atoms H4b and H5b also form moderate hydrogen bonds with the neighbouring water molecules (Ow2 and Ow1) with comparable *D*–H····*A* angles of 168° and 165°, and H····*A* bond distances of 1.826 and 1.858 Å, respectively.

The H6a atom of the Ow6 water molecule (Fig. 4c) forms a hydrogen bond with Cl1, with the interatomic distance 2.109 Å and *D*–H···*A* angle 174°. The H6b atom is involved in a typical three-centred asymmetric hydrogen bond, i.e. bifurcated bond (Rozas *et al.*, 1998). The H6b forms two H6b···*A* bonds to O6 and O2 acceptors with bond distances 1.928 and 2.29 Å, respectively (Fig. 4c), the *D*–H···*A* angles are in the range of 121–150°, and the *A*···H···*A* angle has a value of 83°. Rozas *et al.* (1998) reported that hydrogen bonds become longer in the three-centred type compared to the regular ones, due to the equal sharing of electron density between the H atom and two acceptors. A very sensitive criterion for confirming a three-centred character of hydrogen bonds has been proposed by Taylor *et al.* (1984). This criteria comprises the fact that the hydrogen atom is within 0.2 Å out of the plane defined by *D*, *A* and *A*'. In our case, this value is 0.19 Å.

The water molecule Ow7 is not connected to any of the MgO$_n$(H$_2$O)$_m$ octahedra (Fig. 4d). According to Hawthorne (1992), the Ow7 molecule can be described as an interstitial (H$_2$O)^0 group, bonded to an interstitial cation (potassium). The H7a atom forms a hydrogen bond to Cl1 with a *D*–H···*A* angle
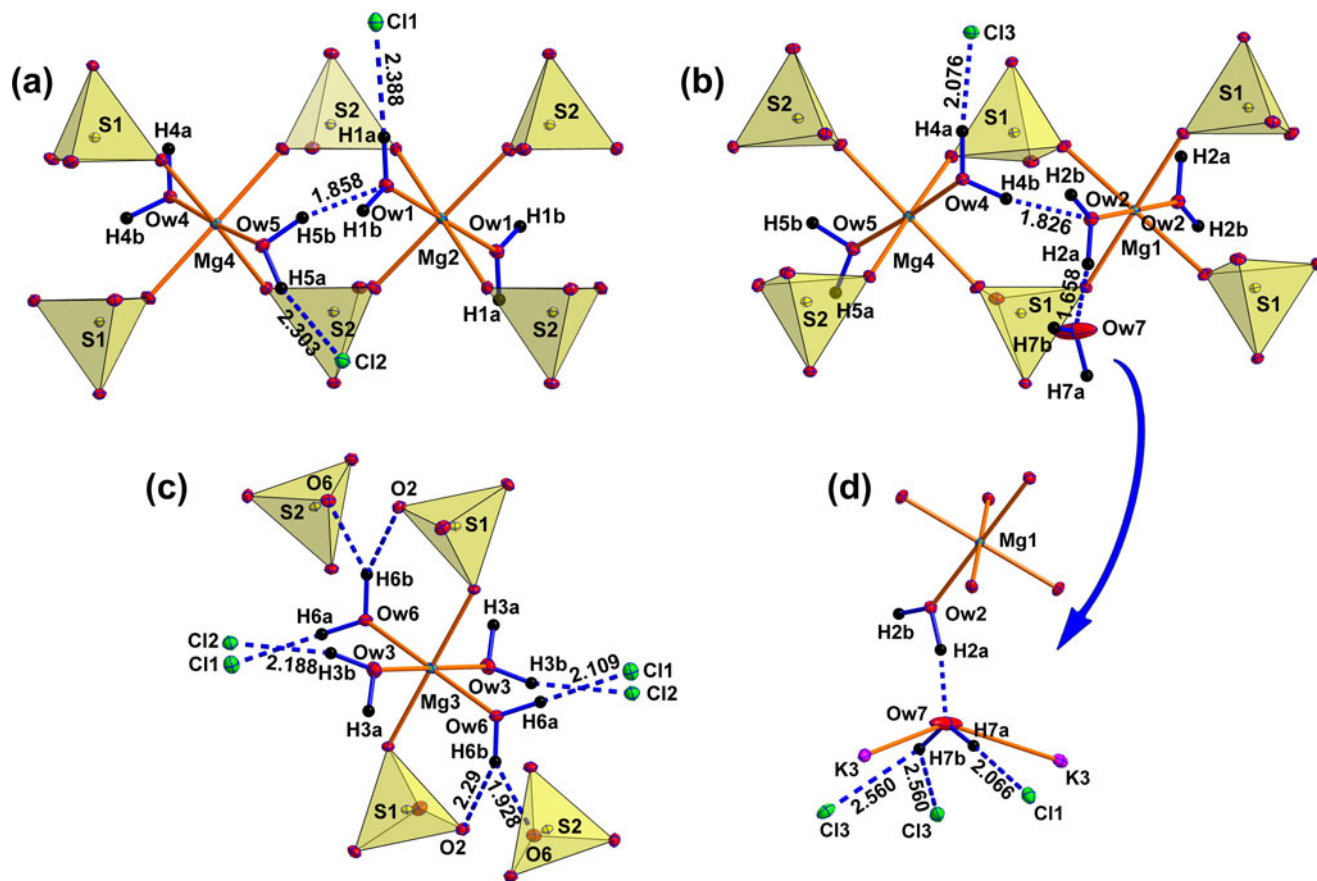
Fig. 4. Environments of the all water molecules in the crystal structure of kainite. Hydrogen *D–A* bonds are shown by blue dotted lines.
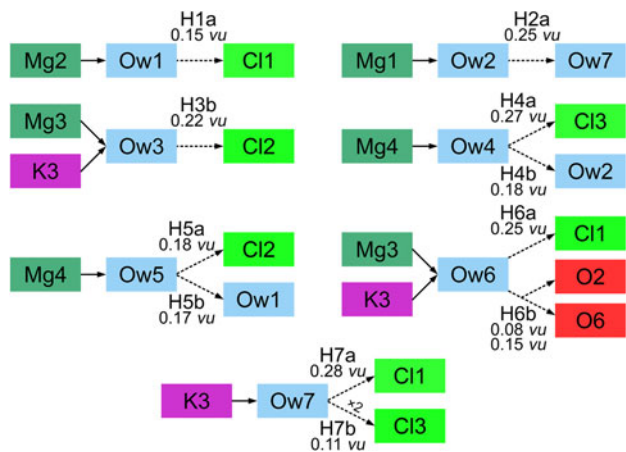

Fig. 5. Schematic representation of hydrogen bonding in kainite.

of 177° and *H*⋯*A* distance of 2.066 Å. The H7b hydrogen forms weak symmetrical hydrogen bonds with two Cl3 atoms as acceptors with a distance of 2.560 Å and *D*–H⋯*A* angle of 133.3°.

Thermogravimetry and differential scanning calorimetry

The results of TG methods (thermogravimetry, TG and differential thermogravimetry, DTG) and DSC studies along with mass spectrometry at *m/z* = 18 are represented in Fig. 6. The TG and

DTG curves exhibit several stages of mass loss. Between 77 and 178°C, the DSC shows a noticeable endothermal effect with a maximum at 155°C which corresponds to a 4.34% mass loss on TG and DTG and can be attributed to the removal of the interstitial Ow7 molecule providing $(H_2O)_{0.25}$ per formula of kainite. The Ow7 water molecule gives 4.50 wt.% to the molecular mass of kainite. The ionic current (IC) at *m/z* = 18 shows a distinct maximum indicating the presence of water vapour in the decomposition products. This endothermal effect is characterised by an absorbed heat of 91.89 J/g. The next, stronger event is observed in the 178–274°C range with a maximum at 222°C which corresponds to the mass loss of 15.18%. The IC curve shows another strong maximum corresponding to release of water vapours. The energetic effect is 323.31 J/g. The overall water loss is 19.52%, whereas the theoretical value for $KMg(SO_4)Cl·2.75H_2O$ is 20.27%.

Between 274 and 320°C the DSC curve exhibits a symmetric exothermal effect with the maximum at 299°C while the TG and IC curves remain featureless. This suggests that a phase transformation is likely to proceed, most probably crystallisation from amorphous or metastable precursors. The effect is characterised by energy of 14.75 J/g.

Between 451 and 560°C, the DSC curve features an endothermal effect with a maximum at 494°C, which is accompanied by a small and long mass loss. This might be caused by melting and slight decomposition. The energy of this effect is 19.48 J/g.

Further heating from 560 to 600°C is characterised by a featureless DSC curve while TG and DTG reflect the last smeared
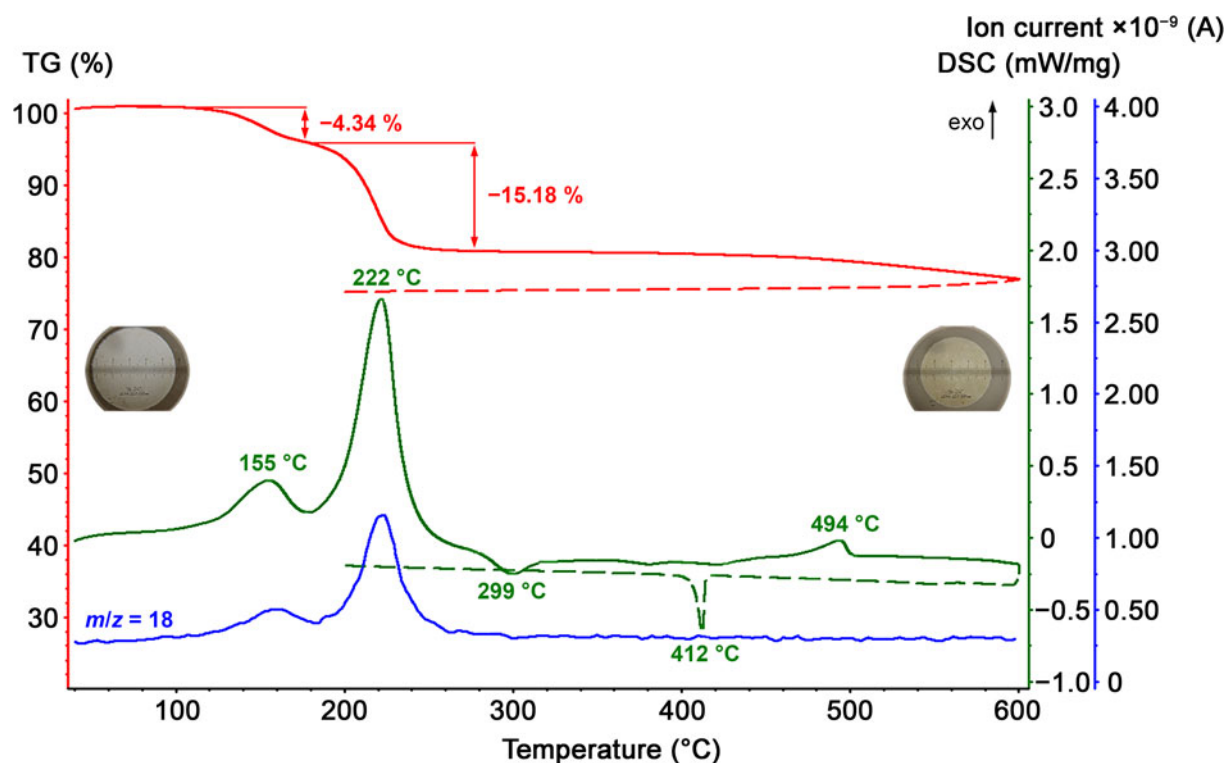
Fig. 6. TG, DSC and IC curves for kainite and *in situ* photographs of the sample before (left) and after (right) heating/cooling cycle. Note the colour change of the probe during the experiment, as well as the decrease of the size of the tablet.

step of mass loss. The IC curve was also featureless which indicates that the decomposition products have probably condensed above 195°C before entering the quadrupole mass spectrometer.

Upon cooling from 600 to 200°C the TG curve shows weak mass losses down to 395°C, while DSC indicates a strong exothermal effect between 417 and 395°C centred at 412°C, probably crystallisation of the melt. The energetic effect is 11.72 J/g.

Thermal evolution of kainite

Variable-temperature powder XRD patterns (Fig. 7) were registered with a step of 5°C between −150°C and 90°C, and with a step of 10°C between 90°C and 600°C.

Between −150°C and 200°C the patterns contain the diffraction maxima of kainite though the trend in their relative position changes abruptly at ~100°C. This can be correlated with the mass loss effect at 155°C (considering the different heating rates for the variable temperature powder XRD and DSC/DTA/MS runs), which corresponds to *ca.* −10.2 g/mol kainite and can be associated roughly with a loss of 0.65–0.75H_2O. At 200°C, further dehydration causes amorphisation until re-crystallisation starts at *ca.* 280°C. From this point on, langbeinite $K_2Mg_2(SO_4)_3$ (Mereiter, 1979) is formed which persists until the highest temperature (600°C) Potassium chloride (Lesly Fathima *et al.*, 2012) is observed between 340°C and 560°C, which is replaced by α-K_2SO_4 (Arnold *et al.*, 1981).

The first loss of water is associated with a distinct shift of the diffraction maxima of kainite which is observed from 110°C and persists until 180°C (before full amorphisation of the sample). In the meantime, no such shift is observed for the benchmark reflections of the Pt-Rh holder. It is most likely that this shift is caused by loss of some water while the overall structure motif is

retained. Unfortunately, the quality of the XRD patterns (particularly the broad lines due to lowered crystallinity) did not permit us to investigate the structural changes which mainly concern the weakest scatterers (O and H). Interstitial Ow7 water molecules are released first. The loss of water and increasing temperature are expected to influence the unit-cell volume in the opposite directions which is manifested by the shift of diffraction maxima. One may speculate that the hypothetical 'anhydrokainite' might actually correspond to the partially dehydrated kainite, or $KMg(SO_4)Cl\cdot(2\pm\delta)H_2O$ (where $\delta \approx 0.1$).

The total dehydration results in decomposition of kainite and formation of an amorphous sample that crystallises into synthetic langbeinite and, at higher temperatures, potassium chloride. The tentative reaction at the first step might be written as $3KMg(SO_4)Cl\cdot2.75H_2O \rightarrow 8.25H_2O\uparrow + K_2Mg_2(SO_4)_3 + KMgCl_3$ (or $KCl + MgCl_2$). While magnesium chloride is rather sensitive to the thermal hydrolysis, its thermal behaviour in the presence of alkali chlorides is more complex and hydrolysis is somewhat retarded or even suppressed (Shoval and Yariv, 1985; Shoval *et al.* 1986). Unfortunately, this behaviour has been studied only by DTG and IR spectroscopy, and it was not reported whether the intermediate products are amorphous or crystalline. The effect at 475°C reported for $KMgCl_3$ which might correspond to crystallisation (Shoval and Yariv, 1985) was not observed in our study. Yet, successive formation of KCl and K_2SO_4 indicates that further exchange processes take place, probably with participating amorphous intermediates, after full decomposition of the initial kainite. In a test experiment, preheated KCl and anhydrous $MgSO_4$ were annealed in a silica-jacketed alumina crucible at 700°C; large high-quality crystals of synthetic langbeinite were the main product.

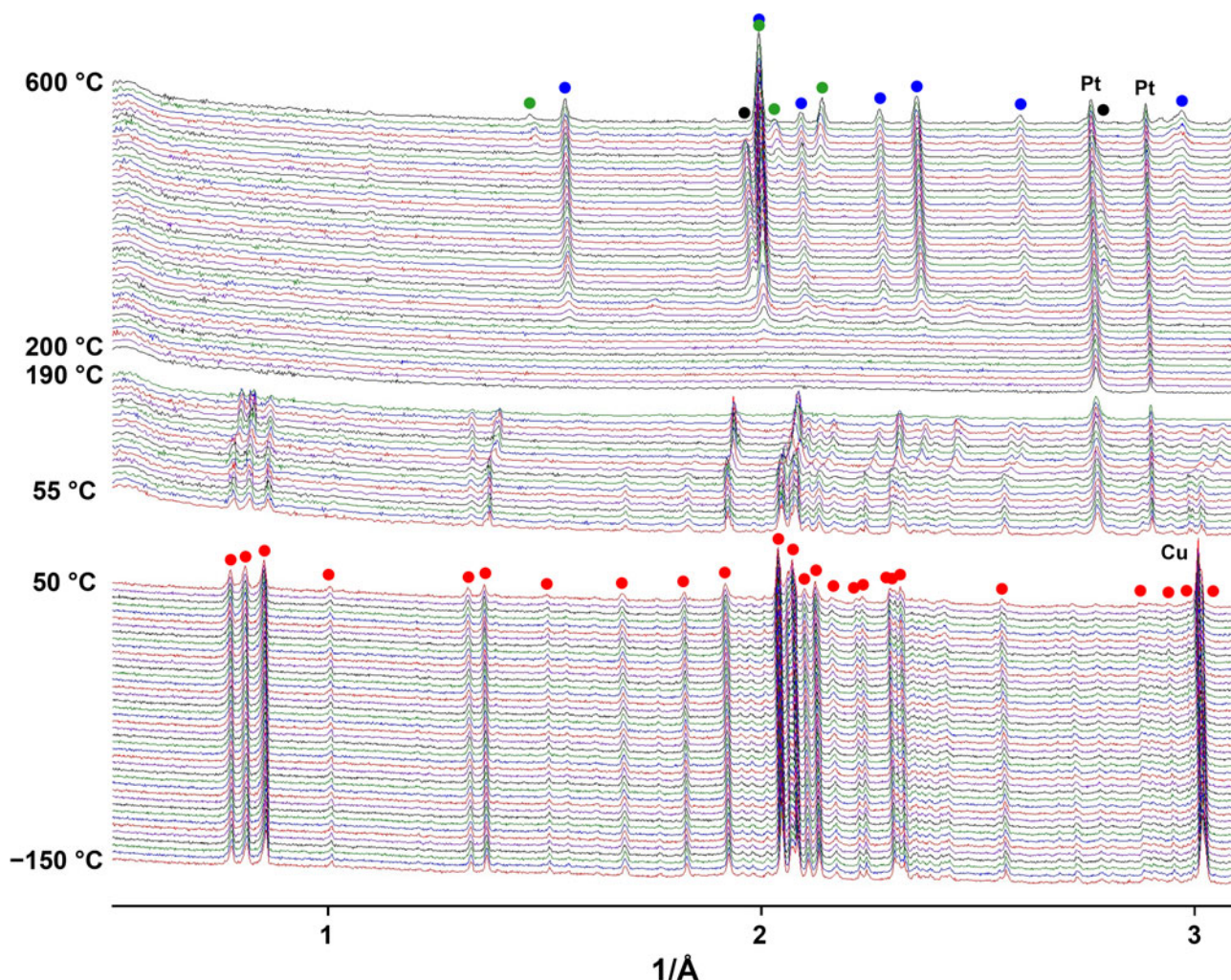The thermal expansion of kainite was studied between −150°C and 50°C wherein the composition $KMg(SO_4)Cl\cdot2.75H_2O$ is

Fig. 7. Evolution of the powder diffraction patterns of kainite as a function of temperature (red circles – kainite, black – KCl, green – K_2SO_4 and blue – langbeinite)

retained. According to the expansion tensor, the largest expansion is observed along α_{33}, while the smallest is along α_{11}, both direction lying in the *ac* plane. The angles of shear deformation are $\mu_c = 47.4°$ for $T = -150$ to $-65°C$; $\mu_c = 47.5°$ for $T = -60$ to $50°C$ ($\mu_c = c^\wedge\alpha_{33}$, the angle between the *c* axis of the unit cell and α_{33} axis of the tensor in the *ac* plane).

It is seen from Fig. 8 that thermal expansion along *c* is less pronounced compared to *a* and *b*. This can be explained keeping in mind that this direction more or less coincides with those of the kröhnkite chains which are relatively rigid. All parameters increase with temperature, according to the equations:

$$a = 19.73792(86) + 0.414(11) \times 10^{-3}\ T\ (\text{Å})$$
$$b = 16.22965(85) + 0.382(12) \times 10^{-3}\ T\ (\text{Å})$$
$$c = 9.53220(48) + 0.2680(64) \times 10^{-3}\ T\ (\text{Å})$$
$$\beta = 94.9279(37) + 0.444(49) \times 10^{-3}\ T\ (°)$$
$$V = 3042.18(23) + 217(3) \times 10^{-3}\ T\ (\text{Å}^3)$$

The behaviour the thermal expansion tensor is typical for monoclinic crystals (Filatov *et al.*, 1984) exemplifying the shear thermal deformations which cause the change of the β angle, according to the equation $\alpha_\beta = (1/\beta)/(d\beta/dT)$.

Concluding remarks

The thermal studies of kainite $KMg(SO_4)Cl\cdot2.75H_2O$ in the temperature range of -150 to $600°C$ indicate its stability until $190°C$, which generally agrees with the results of Bish and Scanlan (2006). The decomposition products are $K_2Mg_2(SO_4)_3$ (Mereiter, 1979), KCl (Lesly Fathima *et al.*, 2012) and K_2SO_4 (Arnold *et al.*, 1981).

As noted above, there remains an unanswered question connected with kainite, namely the possible existence of its anhydrous analogue, 'anhydrokainite' $KMg(SO_4)Cl$. This question was addressed several times in the previous century (Jänecke, 1912; Kassner, 1958 and references therein). To handle it properly from the crystal chemical viewpoint, it is necessary to compare kainite with some chemically related minerals. However, now it is a unique representative of hydrous sulfate chlorides of Group 1 to Group 2 elements. Therefore, these comparisons are possible only with chemically more distant and well characterised species. Note that no structural, or even X-ray data, were reported for the crystals of the claimed-to-be zinc analogue of kainite (Narasimhulu *et al.*, 2000); given the high solubility of zinc halides and relatively low solubility of picromerite-like double sulfates, the identity of crystals grown from solution needs further
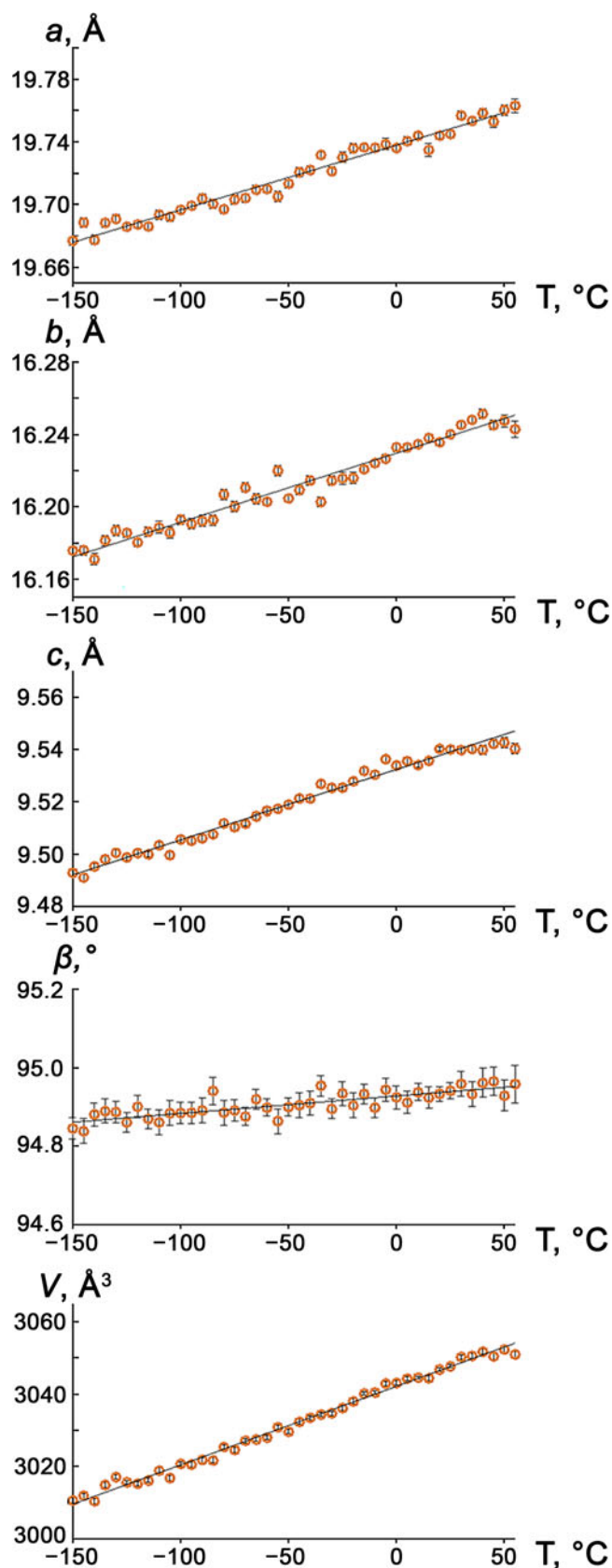
Fig. 8. Temperature dependences of the unit-cell parameters and volume for kainite

verification. According to Narasimhulu *et al.* (2000), partial substitution of Cu^{2+} for Zn^{2+} results in formation of two crystallographically distinct paramagnetic centres which does not correlate with the presence of four symmetrically independent Mg^{2+} sites in the structure of kainite. Our attempts to grow crystals of any Zn-bearing kainite analogues from aqueous solutions were not successful. In the meantime, zinc contributes to a formal analogue of 'anhydrokainite', namely belousovite $KZn(SO_4)Cl$ (Siidra *et al.*, 2018). However, the coordination of Zn^{2+} in its structure is tetrahedral which is uncommon for Mg^{2+} and has not been reported in sulfate minerals to date.

Considering the important role of hydrogen bonds, and chlorine in particular as their acceptor, in the structures of hydrous minerals, it is of interest to compare details with a few other hydrated sulfate chloride minerals and kainite. These structures can be quite conveniently described in terms of structural units and interstitial complexes (Hawthorne, 2015): adranosite $(NH_4)_4NaAl_2(SO_4)_4Cl(OH)_2$ (Demartin *et al.*, 2010) and gordaite $NaZn_4(SO_4)(OH)_6Cl \cdot 6H_2O$ (Zhu *et al.*, 1997). In both of these minerals chloride contributes to the components of structural units (infinite $\cdots Na–Cl–Na–Cl\cdots$ chains in adranosite and coordination environment of Zn in gordaite). In the case of adranosite the large cavities occupied by nine-coordinated NH_4^+ ions, and chlorine from structural unit acts as an acceptor for hydrogen bonding. In the structure of gordaite the zinc hydroxide layers are held together by a system of hydrogen bonds from the hexaaquo Na^+ ions to oxygen and chlorine atoms from the structural unit.

The structure of kainite exhibits some particularities. Chloride is not coordinated to magnesium, hence it does not contribute to the formation of structural units, but rather bonds to potassium cations within interstitial complexes. The major role of the chloride anions in the structure of kainite is accepting hydrogen bonds from various water molecules. As a result, we observe a complex network of hydrogen bonds, including not only the regular hydrogen bonds, but also three-centre and symmetric ones. Therefore, the hypothetical anhydrous compound $KMg(SO_4)Cl$, if it exists, would be highly likely to adopt a quite different arrangement. However, the kainite structure probably tolerates loss of ca. 30% of water molecules; therefore, the 'anhydrokainite' might actually be this partially dehydrated species. It is also possible that the amorphous intermediate obtained at ~200°C might have become crystalline over a long time, which is very much possible under natural conditions.

References

Abdel Wahed M.S.M., Mohamed E.A., El-Sayed M.I., M'nif A. and Sillanpää M. (2015) Crystallization sequence during evaporation of a high concentrated brine involving the system Na–K–Mg–Cl–SO$_4$–H$_2$O. *Desalination*, **355**, 11–21.

Arnold H., Kurtz W., Richter-Zinnius A., Bethke J. and Heger G. (1981) The phase transition of K_2SO_4 at about 850 K. *Acta Crystallographica*, **B37**, 1643–1651.

Babel M. and Schreiber B.C. (2014) Geochemistry of evaporites and evolution of seawater. Pp. 483–560 in: *Treatise on Geochemistry*, 2nd ed., vol. 9. (H.D. Holland and K.K. Turekian, editors). Elsevier, Oxford, UK.

Barlow N. (2008) *Mars: An Introduction to its Interior, Surface and Atmosphere*. Cambridge University Press, Cambridge, UK, 286 pp.

Bish L. and Scanlan M.K. (2006) The hydration and dehydration of hydrous mixed-cations. *Lunar and Planetary Science XXXVII*, Extended abstract 1011 [available at https://www.lpi.usra.edu/meetings/lpsc2006/pdf/1011.pdf].

Braitsch O. (1971) *Salt Deposits: Their Origin and Composition*. Springer, Berlin, 299 pp.

Bruker (2014) *Topas 5.0. General profile and structure analysis software for powder diffraction data*. Bruker A.X.S., Karlsruhe, Germany.

Bubnova R.S., Firsova V.A. and Filatov S.K. (2013) Software for determining the thermal expansion tensor and the graphic representation of its characteristic surface (ThetaToTensor-TTT). *Glass Physics and Chemistry*, **39**, 347–350.

Campbell A.N., Downes K.W. and Samis C.S. (1934) The system $MgCl_2$–KCl–$MgSO_4$–K_2SO_4–H_2O at 100°. *Journal of the American Chemical Society*, **56**, 2507–2512.

Censi P., Sposito F., Inguaggiato C., Venturi M., Censi V. and Falcone E.E. (2016) Weathering of evaporites: natural versus anthropogenic signature on the composition of river waters. *Rendiconti Lincei*, **27**, 29–37.

Chukanov N.V. (2014) *Infrared Spectra of Mineral Species: Extended library*. Springer Dordrecht Heidelberg New York London, 1726 pp.

Demartin F., Gramaccioli C.M. and Campostrini I. (2010) Adranosite, $(NH_4)_4NaAl_2(SO_4)Cl(OH)_2$, a new ammonium sulfate chloride from La Fossa crater, Vulcano, Aeolian Islands, Italy. *The Canadian Mineralogist*, **48**, 315–321.

Dhanuskodi S. and Jeyakumari A.P. (2001) EPR studies of VO^{2+} ions in kainite single crystals. *Spectrochimica Acta Part A: Molecular and Biomolecular Spectroscopy*, **57**, 971–975.

Dhanuskodi S. and Jeyakumari A.P. (2004) EPR studies of Cr^{3+} ions in kainite single crystals. *Materials Chemistry and Physics*, **87**, 292–296.

Eggenkamp H.G.M., Kreulen R. and Koster Van Groos A.F. (1995) Chlorine stable isotope fractionation in evaporites. *Geochimica et Cosmochimica Acta*, **59**, 5169–5175.

Eugster H.P, Harvie C.E. and Weare J.H. (1980) Mineral equilibria in a six-component seawater system, Na–K–Mg–Ca–SO_4–Cl–H_2O, at 25°C. *Geochimica et Cosmochimica Acta*, **44**, 1335–1347.

Lesly Fathima A., Sivananthan S., Somasundari C.V. and Neelakandapillai N. (2012) X-ray diffraction and micro hardness measurement on $KCl_xBr_{1−x}$ single crystals doped with ZnO grown from aqueous solution. *Archives of Physics Research*, **3**, 407–410.

Filatov S.K., Andrianova L.V. and Bubnova R.S. (1984) Regularities of thermal deformations in monoclinic crystals. *Crystal Research and Technology*, **19**, 563–569.

Fleck M., Kolitsch U. and Hertweck B. (2002) Natural and synthetic compounds with kröhnkite-type chains: review and classification. *Zeitschrift für Kristallographie*, **217**, 435–443.

Gagné O.C. and Hawthorne F.C. (2015) Comprehensive derivation of bond-valence parameters for ion pairs involving oxygen. *Acta Crystallographica*, **B71**, 562–578.

Gagné O.C. and Hawthorne F.C. (2016) Bond-length distributions for ions bonded to oxygen: alkali and alkaline-earth metals. *Acta Crystallographica*, **B72**, 602–625.

Gagné O.C. and Hawthorne F.C. (2018) Bond-length distributions for ions bonded to oxygen: results for the non-metals and discussion of lone-pair stereoactivity and the polymerization of PO_4. *Acta Crystallographica*, **B74**, 79–96.

Hancer M. and Miller J.D. (2000) The flotation chemistry of potassium double salts: Schoenite, kainite, and carnallite. *Minerals Engineering*, **13**, 1483–1493.

Hawthorne F.C. (1992) The role of OH and H_2O in oxide and oxysalt minerals. *Zeitschrift für Kristallographie*, **201**, 183–206.

Hawthorne F.C. (2015) Toward theoretical mineralogy: A bond-topological approach. *American Mineralogist*, **100**, 696–713.

Hawthorne F.C., Burns P.C. and Krivovichev S.V. (2000) The crystal chemistry of sulfate minerals. Pp. 1–112 in: *Sulfate Minerals – Crystallography, Geochemistry and Environmental Significance* (PH Riibe, editor). Reviews in Mineralogy and Geochemistry, 40. Mineralogical Society of America and the Geochemical Society, Chantilly, Virginia, USA.

Hryniv S., Parafiniuk J. and Peryt T.M. (2007) Sulphur isotopic composition of K–Mg sulphates of the Miocene evaporites of the Carpathian Foredeep, Ukraine. Pp. 265–273 in: *Geological Society, London, Special Publications*, Vol. 285 (B.C. Schreiber, S. Lugli and M. Bąbel, editors). The Geological Society of London, UK.

Jänecke E. (1912) Über reziproke Salzpaare. II. *Zeitschrift für Physikalische Chemie*, **80U**, 1–12.

Jena S.K. (2021) A review on potash recovery from different rock and mineral sources. *Mining, Metallurgy and Exploration*, **38**, 47–68.

Kassner B. (1958) Die Bildung von Kainit im Ultraschallfeld als Festkörperreaktion und Untersuchungen über den Anhydrokainit. *Zeitschrift für anorganische und allgemeine Chemie*, **297**, 139–145.

Kresse G. and Furthmüller J. (2017) *Vienna Ab-initio Simulation Package (VASP)*, v.5.4.4. VASP Software GmbH, Vienna.

Kresse G. and Joubert D. (1999) From ultrasoft pseudopotentials to the projector augmented-wave method. *Physical Review B*, **59**, 1758.

Mereiter K. (1979) Refinement of the crystal structure of langbeinite $K_2Mg_2(SO_4)_3$. *Neues Jahrbuch fuer Mineralogie, Monatshefte*, 182–188.

Miller J.D. and Yalamanchili M.R. (1994) Fundamental aspects of soluble salt flotation. *Minerals Engineering*, **7**, 305–317.

Murthy T.S.N., Srinivas V., Dayanand C. and Salagram M. (1992a) EPR Spectra of SO_4^- centres in X-irradiated kainite ($KMgSO_4·3H_2O$) crystals. *Physica Status Solidi (a)*, **133**, K33–K36.

Murthy T.S.N., Srinivas V., Dayanand C. and Salagram M. (1992b) EPR characterisation of SO_3^- radical in X-irradiated kainite ($KMgClSO_4·3H_2O$) crystals. *Solid State Communications*, **84**, 673–677.

Narasimhulu K.V., Sunandana C.S. and Rao J.L. (2000) Electron paramagnetic resonance studies of Cu^{2+} ions in $KZnClSO_4·3H_2O$: an observation of Jahn–Teller distortion. *Journal of Physics and Chemistry of Solids*, **61**, 1209–1215.

Nazzareni S., Comodi P. and Hanfland M. (2018) High-pressure single-crystal synchrotron X-ray diffraction of kainite ($KMg(SO_4)Cl·3H_2O$). *Physics and Chemistry of Minerals*, **45**, 727–743.

Pasero M (2022) *The New IMA List of Minerals*. http://cnmnc.main.jp/

Pekov I.V., Zubkova N.V., Belakovskiy D.I., Lykova I.S., Yapaskurt V.O., Vigasina M.F., Sidorov E.G. and Pushcharovsky D.Yu. (2015) Sanguite, $KCuCl_3$, a new mineral from the Tolbachik volcano, Kamchatka, Russia. *The Canadian Mineralogist*, **53**, 633–641.

Rao S.N., Vedanand S., Ravikumar R., Ravikumar R.V.S.S.N. and Reddy Y.P. (1994) Optical absorption spectra of cobalt and nickel doped kainite. *Solid State Communications*, **92**, 815–819.

Rice M.S., Bell J.F. III, Cloutis E.A., Wang A., Ruff S.W., Craig M.A., Bailey D.T., Johnson J.R., De Souza Jr. P.A and Farrand W.H. (2010) Silica-rich deposits and hydrated minerals at Gusev Crater, Mars: Vis-NIR spectral characterization and regional mapping. *Icarus*, **205**, 375–395.

Rigaku (2016) *PDXL: Integrated X-ray Powder Diffraction Software*. Rigaku Corporation, Oxford, UK.

Rigaku (2021) *CrysAlisPro Software System Version 1.171.41.103a*. Rigaku Corporation, Oxford, UK.

Robinson P.D., Fang J.H. and Ohya Y. (1972) The crystal structure of kainite. *American Mineralogist*, **57**, 1325–1332.

Rozas I., Alkorta I. and Elguero J. (1998) Bifurcated hydrogen bonds: three-centered interactions. *Journal of Physical Chemistry A*, **102**, 9925–9932.

Salagram M., Seetharam K., Siddambary P. and Murthy T.S.N. (1988) Infrared characterisation of the oxyanion in kainite. *Physica Status Solidi (a)*, **106**, K185–K190.

Salagram M., Madhukar K., Murthy T.S.N. and Sunandana C.S. (1994) ESR characterisation of SO_3^- and SO_4^- radicals in X-irradiated kainite ($KMgClSO_4·3H_2O$). *Spectrochimica Acta*, **A50**, 1309–1315.

Sheldrick G.M. (2015) Crystal structure refinement with SHELXL. *Acta Crystallographica*, **C71**, 3–8.

Shields G.A. and Mills B.J.W. (2021) Evaporite weathering and deposition as a long-term climate forcing mechanism. *Geology*, **49**, 299–303.

Shoval S. and Yariv S. (1985) The effect of alkali-chloride on the thermal hydrolysis of hydrated magnesium-chloride. *Thermochimica Acta*, **92**, 819–822.

Shoval S., Yariv S., Kirsch Y. and Peled H. (1986) The effect of alkali halides on the thermal hydrolysis of magnesium chloride and magnesium bromide. *Thermochimica Acta*, **109**, 207–226.

Siidra O.I., Nazarchuk E.V., Lukina E.A., Zaitsev A.N. and Shilovskikh V.V. (2018) Belousovite, KZn(SO$_4$)Cl, a new sulfate mineral from the Tolbachik volcano with apophyllite sheet-topology. *Mineralogical Magazine*, **82**, 1079–1088.

Spencer R.J. (2000) Sulfate minerals in evaporite deposits. Pp. 173–192 in: *Sulfate Minerals – Crystallography, Geochemistry and Environmental Significance* (PH Riibe, editor). Reviews in Mineralogy and Geochemistry, 40. Mineralogical Society of America and the Geochemical Society, Chantilly, Virginia, USA.

Steiner T. (2002) The hydrogen bond in the solid state. *Angewandte Chemie International Edition*, **41**, 48–76.

Subramanian P. and Hariharan N. (1986) Electron paramagnetic resonance study of Mn^{2+} in kainite. *Pramana*, **26**, 555–560.

Sun J., Ruzsinszky A. and Perdew J.P. (2015) Strongly constrained and appropriately normed semilocal density functional. *Physical Review Letters*, **115**, 036402.

Taylor R., Kennard O., and Versichel W. (1984) Geometry of the nitrogen–hydrogen⋯oxygen–carbon (N–H⋯O:C) hydrogen bond. 2. Three-center (bifurcated) and four-center (trifurcated) bonds. *Journal of American Chemical Society*, **106**, 244–248.

Wang H.-Y., Guo H.-M., Xiu W., Bauera J., Sun G.-X., Tang X.-H. and Norra S. (2019) Indications that weathering of evaporite minerals affects groundwater salinity and As mobilization in aquifers of the northwestern Hetao Basin, China. *Applied Geochemistry*, **109**, 104416.

Warren J.K. (2010) Evaporites through time: Tectonic, climatic and eustatic controls in marine and nonmarine deposits. *Earth-Science Reviews*, **98**, 217–268.

Zhu L., Seff K., Witzke T. and Nasdala L. (1997) Crystal structure of Zn$_4$Na(OH)$_6$SO$_4$Cl·6H$_2$O. *Journal of Chemical Crystallography*, **27**, 325–329.

Zincken C. (1865) Ueber ein neues salz von Leopoldshall bei Stassfurth. *Berg- und Huttenmannische Zeitung*, **24**, 79–80.